Delft University of Technology

# Influence of Residual Dyke Strength on Dyke Reliability Using the Random Material Point Method

Remmerswaal, Guido; Hicks, Michael; Vardon, Phil

**DOI**
10.3850/978-981-11-2725-0 IS4-4-cd

**Publication date**
2019

**Document Version**
Final published version

**Published in**
Proceedings of the 7th International Symposium on Geotechnical Safety and Risk (ISGSR 2019)

# Influence of Residual Dyke Strength on Dyke Reliability Using the Random Material Point Method

Guido Remmerswaal[1], Michael A. Hicks[2], and Philip J. Vardon[3]

[1]Geo-Engineering Section, Delft University of Technology, Delft, the Netherlands.
E-mail: g.remmerswaal@tudelft.nl
[2]Geo-Engineering Section, Delft University of Technology, Delft, the Netherlands. E-mail: m.a.hicks@tudelft.nl
[3]Geo-Engineering Section, Delft University of Technology, Delft, the Netherlands. E-mail: p.j.vardon@tudelft.nl

**Abstract:** The material point method (MPM) is used to model both rotational and horizontal sliding failure mechanisms of dykes under external (water) loading. To model the different failure mechanisms, an external hydrostatic water pressure has been applied on the canal side of the dyke by applying a newly developed boundary condition. The boundary condition detects the material boundary and distributes the applied load to the nodes of the background mesh. The definition of dyke failure has also been investigated using MPM. In conventional dyke assessment, using (for example) the finite element method (FEM), the dyke is considered to have failed as soon as an initial failure occurs. However, the dyke may still be able to resist the flow of water, and this continuing ability to resist water flow is known as residual dyke strength. By taking account of residual dyke strength, for example with MPM as shown in this paper, the computed reliability can increase compared to conventional assessment, as in some cases total dyke failure does not occur after an initial slope failure. Finally, spatial variability is considered using the random material point method (RMPM), which combines random fields with MPM in a Monte Carlo framework. When considering spatial variability, a significant gain in reliability due to residual dyke strength has been observed, but further investigation is required to fully understand the effect of spatial variability on residual dyke strength. In order to simplify this preliminary investigation, the adopted soil properties in this paper have not been based on actual soils used in dyke construction; the results are only intended to indicate the capabilities of RMPM and develop hypotheses on the effect of residual dyke strength.

Keywords: Dyke breach; dyke reliability; residual strength; RMPM; ultimate limit state.

## 1 Introduction

This paper continues the investigation of Wang et al. (2016) and Remmerswaal et al. (2018) into the influence of residual dyke strength on dyke reliability. Generally, in dyke assessments, inner slope instability (macro-instability) is considered as failure of a dyke. However, several dyke slope failures have been observed which did not result in flooding ('t Hart et al. 2016); i.e., the dyke had residual strength. In the Netherlands, flooding is considered to be the ultimate limit state (ULS) of dykes, but residual dyke strength is generally not accounted for in the Dutch assessment guide for macro-instability (MIM 2016), as a clear method to assess this strength is unavailable. In specific cases, where a dyke is considered unsafe based on an assessment of inner slope instability alone, the geometry after the initial slope failure can been used to approximate residual strength (MIM 2016). In this case, a dyke is assumed to have residual dyke strength, as well as a lower probability of flooding, when, after the initial failure, the dyke has a considerable width and height compared to the expected water level.

This work continues the development and application of the random material point method (RMPM), which can be used to compute both the probability of initial slope failure as well as the probability of flooding (regarding macro-instability). The material point method (MPM) is a recent extension of the finite element method (FEM), which removes the effect of mesh distortion by decoupling the material from the finite element mesh and discretizing the material as an assembly of points (Sulsky et al. 1994). The material points within the model flow through the mesh, thereby extending FEM to large deformation modelling. RMPM combines MPM with random fields of material properties, which are mapped onto the material points and used in a Monte Carlo simulation to compute the reliability of structures based on large deformations. Compared to previous analyses involving residual dyke strength with this method (Remmerswaal et al. 2018), this paper includes an external hydrostatic pressure on the outer slope of the dyke, thereby preventing failure of the outer slope. This external pressure improves the applicability of the method and the resemblance to reality.

In two short sections, RMPM and the application of an external hydrostatic pressure are outlined. A deterministic MPM is then used to model a simplified dyke, which experiences either a horizontal rupture or rotational failure mechanism. Finally, the same dyke is modelled with RMPM to investigate the effect of spatial variability and residual dyke strength on the dyke failure, and to compute the reliability of a simplified dyke.

## 2 Random Material Point Method

*Proceedings of the 7th International Symposium on Geotechnical Safety and Risk (ISGSR)*
*Editors:* Jianye Ching, Dian-Qing Li and Jie Zhang

*Published by* Research Publishing, Singapore.
ISBN: 978-981-11-2725-0; doi:10.3850/978-981-11-2725-0_IS4-4-cd

In MPM, all variables, such as stress, strain, displacement, velocity, mass and strength, are stored at the material points. Within each time step the required variables are mapped to the nodes of the background grid, after which the governing equations of FEM are solved at the nodes. In this paper an implicit MPM formulation has been used, including some optimization strategies to reduce stress oscillations as mentioned by Gonzalez Acosta et al. (2017). At the end of each time step, the nodal variables are used to update the material point variables.

The version of MPM used in this work performs a total stress analysis under undrained conditions with a strain softening Von Mises constitutive model. The strain softening represents the loss in strength due to the build-up of excessive pore pressure during deformation. In future research effective stresses will be incorporated within this model, but the current model already provides insight into the expected behavior.

The initial and residual cohesions, $c_i$ and $c_r$, respectively, of each material point are based on generated fully correlated random fields. Each Monto Carlo simulation uses multiple realizations, in which a different random field is mapped onto the material points in each realization. This concept is similar to the random finite element method (RFEM), where random fields are mapped to the Gauss points. RFEM has proven to be a useful tool to compute the reliability against initial slope failure (Griffiths et al. 2009; Varkey et al. 2018). The random fields are created based on the probability distributions, on the point statistics, i.e. mean and coefficient of variation, and on the correlation functions, i.e. horizontal and vertical scales of fluctuation, $\theta_h$ and $\theta_v$, respectively.

## 3 External Hydrostatic Pressure

Applying external boundary conditions in MPM is rather difficult, as the boundary is no longer defined by the finite element mesh (Remmerswaal 2017; Bing et al. 2019). Moreover, as the material points are centers of mass, they cannot be used to represent the boundary. The authors therefore developed a new method which transfers external loads to the nodes, similar to FEM, to be able to solve the FEM governing equations.

In FEM a boundary condition is distributed over the nodes of the boundary of the mesh, which is given by a line in 2D. The same concept is used in this new method, as it uses FEM shape functions to distribute the load from the material boundary to the nodes. However, as the location of the boundary is unknown, an edge detection method has been developed to locate the boundary based on the position of the material points. The method is based on a contour algorithm applied on a field of kernel functions surrounding the material points. More details on the detection algorithm can be found in Remmerswaal (2017). Linear segments are used here to define the boundary. A hydrostatic water pressure is applied normal to this boundary, based on a fixed water level, and Gaussian integration is used to map the load from the boundary to the nodes of the background mesh.

## 4 Problem Description

The RMPM model, including hydrostatic pressure on the canal side, has been tested on a simplified dyke, similar to the dyke presented in Remmerswaal et al. (2018), but now with more realistic boundary conditions as shown in Figure 1. The clay dyke is 10 m high, has a design water level 0.5 m below the 20 m wide crest, and a slope angle of 1:1. The foundation of the dyke is assumed to be rigid, resulting in a fixed bottom boundary condition. The Young's modulus $E$ is 1000 kPa and the unit weight of the material $\gamma$ is 20 kN/m$^3$. The water level is assumed to be constant during the entire simulation and the dyke is assumed to fail in an undrained manner. For simplicity, the dyke has a uniform self-weight and the phreatic surface is not modelled, i.e. the dyke is assumed to be fully saturated. To promote numerical convergence, Poisson's ratio $\nu$ is 0.45. The $c_i$ and $c_r$ vary for each simulation, to cause failure of the dyke, as explained in the upcoming sections. The softening modulus is -50 kPa for all simulations.

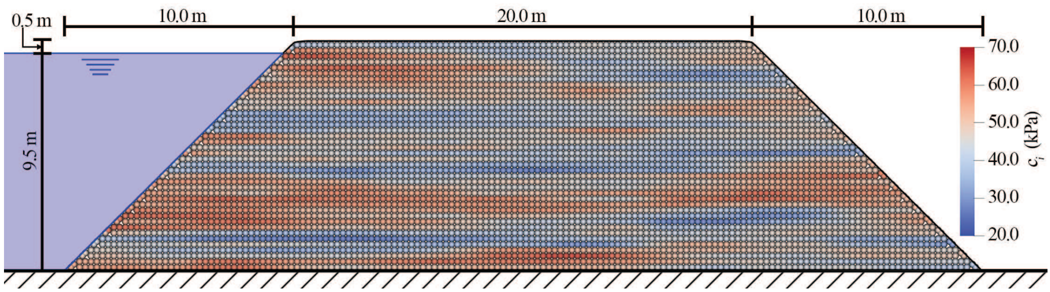


**Figure 1.** Problem description of MPM dyke simulation highlighting a single random field of initial undrained shear strength $c_i$. The random field uses $\theta_v$ = 1.0 m and $\theta_h$ = 24 m.

To generate in-situ stresses the dyke is loaded quasi-statically by gravity with elastic soil properties, after which the stresses of the material points are returned to the yield surface according to the undrained cohesion. The unbalanced nodal loads, caused by the change of stress of the plastic material points, are damped during the first second of the dynamic simulation, which follows the quasi-static in-situ stress generation. During this first second the damping is reduced from 100% to 0% to reduce oscillations caused by the initial condition. The simulations are assumed to finish after the occurrence of flooding, or after 20 seconds, whichever occurs first.

The current simulations are greatly simplified compared to most real dyke failures, due to the simple geometry, the use of total stresses instead of effective stresses, the assumption that the entire dyke has uniform self-weight, the fixed water level and certain unrealistic properties chosen to speed up the simulations. However, these simulations still indicate the capabilities of the general approach, as the upcoming sections highlight that both rotational and horizontal dyke failure mechanisms can be modelled for spatially varying soil strengths.

## 5 Deterministic Horizontal Slide versus Rotational Slope Failure

Due to the application of a hydrostatic pressure on the outer slope, both horizontal and rotational (inner slope) dyke failure mechanisms are possible. The dyke was assumed to be a sensitive clay, to highlight the effect of softening, with the residual cohesion fixed to $c_r$ = 10 kPa. The effect of spatial variability is ignored. The initial cohesion $c_i$ has been varied to find the strength at which different types of failure occur. For the normal unit weight ($\gamma$ = 20 kN/m$^3$) the dyke is stable for any $c_i$ larger than 48 kPa (Figure 2a). An initial rotational failure can be triggered by reducing $c_i$ to 47 kPa as shown in Figure 2b. Due to the fixed bottom boundary condition, homogeneous properties and slope angle, a failure along the bottom boundary is expected. The sensitivity of the clay almost triggers flooding for $c_i$ = 47 kPa, as a retrogressive slip surface starts to develop, but enough residual dyke strength remains. A larger reduction to $c_i$ = 46 kPa, see Figure 2c, leads to flooding, after which the model is terminated as complete dyke failure has occurred. Hence, no residual dyke strength is available in Figure 2c.

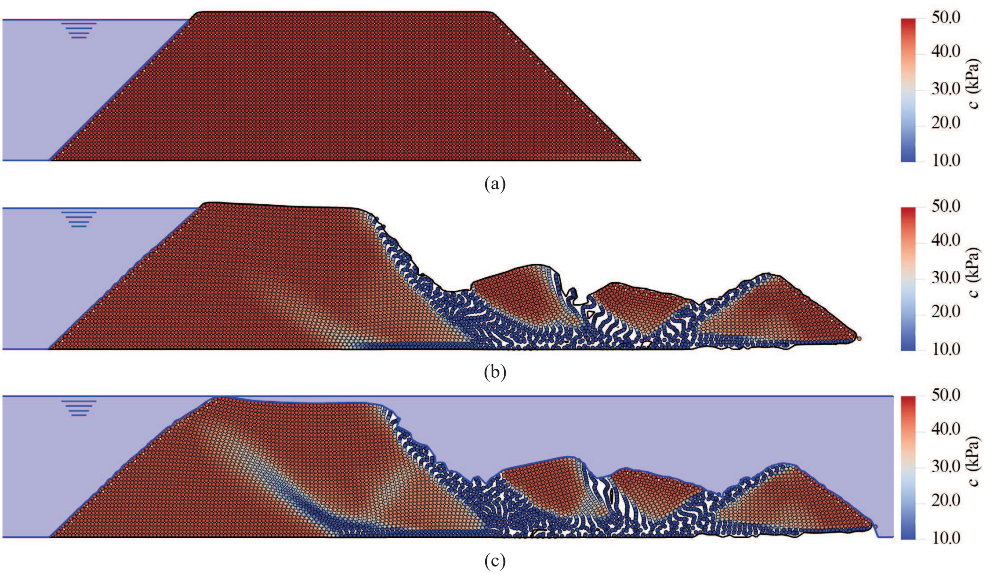


**Figure 2.** Rotational slope failure mechanisms for homogeneous dykes with slightly different initial cohesion: (a) no failure for $c_i$ = 48 kPa; (b) initial slope failure for $c_i$ = 47 kPa; (c) flooding for $c_i$ = 46 kPa.

A dyke failure in Wilnis in 2003 indicated that while rotational slope failure is the most usual macro-instability, for lightweight (usually dry peat) dykes a horizontal sliding mechanism must also be considered (Van Baars 2005). The previous model can easily be adjusted to trigger a horizontal slide instead of a slope failure by lowering the unit weight and strength of the material to resemble a dry peat. Due to the used constitutive model, undrained behavior is still assumed within the dry material. In this case $\gamma$ has been reduced to 5 kN/m$^3$, which triggers a failure for $c_i$ = 15 kPa as shown in Figure 3b. The dyke in Figure 3a has a slightly higher strength ($c_i$ = 16 kPa), which provides insight into the development of the failure mechanism; due to the hydrostatic pressure, a localised failure is starting to develop at the bottom of the dyke from the outer slope towards the inner slope. A full failure did not occur in Figure 3a due to the higher strength, whereas the failure completely developed in

Figure 3b. Once the softening reduced the cohesion to the residual value for the entire bottom of the dyke, it started to slide, first reaching the configuration of Figure 3b, and then continuing to slide until it reached the fixed vertical boundary on the right-hand-side of the simulation domain (not shown in the figure). As the domain is only 2 dimensional, theoretically flooding did not occur as the dyke always remained higher than the water level. However, in the Wilnis failure, this mechanism created two breaches on either side of the slide in the third dimension, so that flooding did occur, i.e. no residual dyke strength was present (Van Baars 2004).

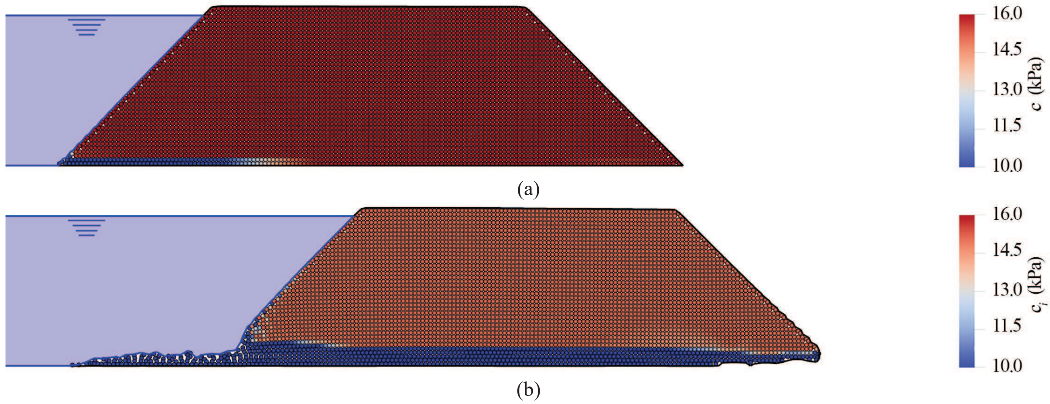


**Figure 3.** Horizontal dyke failure mechanisms for homogeneous dykes with slightly varying initial cohesion: (a) no failure for $c_i$ = 16 kPa; (b) complete failure for $c_i$ = 15 kPa.

## 6 Effect of Residual Dyke Strength on Reliability

As explained earlier, the goal is to investigate the effect of residual dyke strength on the reliability of a dyke with RMPM. Eight Monte Carlo simulations have been performed, with each comprising at least 800 realizations. Each realization within a Monte Carlo simulation uses random fields of initial and residual cohesion based on the same statistics. All simulations use a mean $c_i$ of 48 kPa and a mean $c_r$ of 10 kPa, together with a coefficient of variation of 0.2 for both $c_i$ and $c_r$. The random fields for $c_i$ and $c_r$ are fully correlated. The vertical scale of fluctuation $\theta_v$ is easier to measure than the horizontal scale of fluctuation $\theta_h$, and tends to be small compared to the height of a dyke. Therefore, $\theta_v$ = 1.0 m was assumed in all simulations, whereas $\theta_h$ (1.0, 2.0, 3.0, 4.0, 6.0, 12.0, 24.0 and 48.0 m) is varied to investigate the effect of different amounts of layering in the spatial variability.

For $\theta_h$ = 48.0 m, four realizations are presented in Figures 4 and 5. These indicate some of the failure mechanisms which can be triggered by the presence of weak zones, and shows the importance of spatial variability in predicting both the initial slope failure and ultimate limit state failure of a dyke. Figure 4 shows two realizations which did not result in flooding. Due to a strong layer at the bottom of the inner slope in Figure 4a, slope failure has been prevented entirely. Conversely, slope failure occurs in Figure 4b, due to a slightly weaker material, although the clay was strong enough to prevent a retrogressive failure.

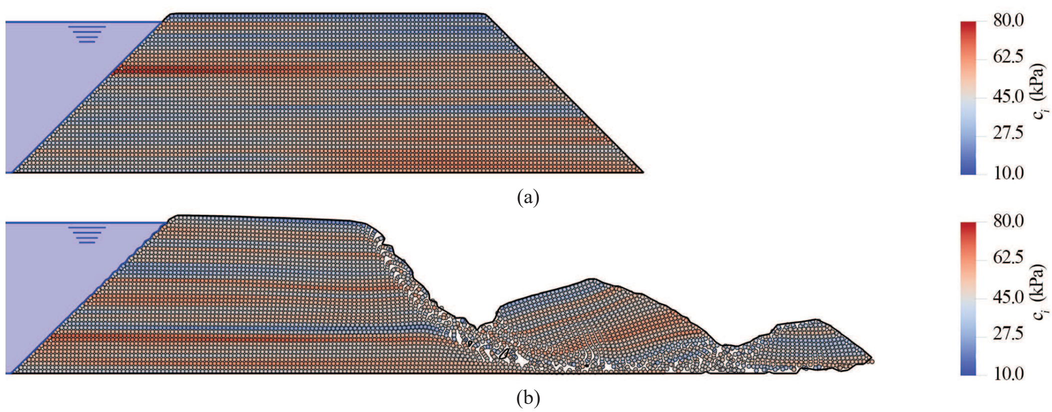


**Figure 4.** Realizations without ULS dyke failure for random fields with $\theta_h$ = 48 m: (a) no initial slope failure; (b) initial failure with enough residual dyke strength to prevent ULS failure.

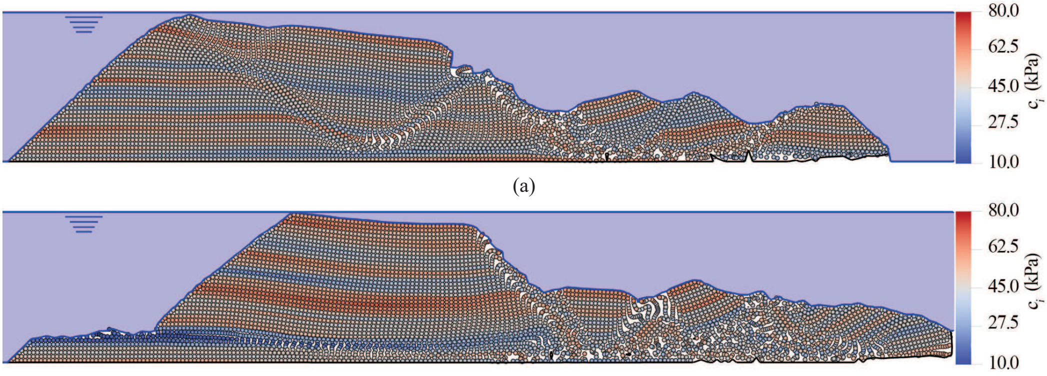


**Figure 5.** Realizations with ULS dyke failure for random fields with $\theta_h$ = 48 m: (a) rotational retrogressive failure; (b) initial slope failure followed by a horizontal slide through a weak layer.

Flooding occurs for the simulations shown in Figure 5, although the two simulations are clearly different. In Figure 5a, an initial slope failure has been triggered, after which softening causes additional rotational failures, eventually leading to complete dyke failure. In Figure 5b, a horizontal failure is partly visible, which is caused by an extremely weak layer approximately 2 meters above the bottom of the dyke. An initial rotational slope failure decreased the effective dyke width, after which the hydrostatic loading was able to overcome the resistance of the weak layer.

The results of the Monte Carlo simulations are summarized in Figures 6 and 7. Figure 6a shows the development, with respect to time, of reliability with respect to initial failure, as could also have been computed using RFEM due to the limited deformations at the onset of the initial failure. As expected, as time progresses initial failure occurs in more realizations. As shown in Figure 7, the reliability against initial failure is lowest for $\theta_h$ = 12 m at ~30 %. Taking the residual strength of the dyke into account clearly has a positive influence on the reliability against ULS failure, see Figures 6b and 7. The reliability increases by at least 30% when considering the residual strength, with the ULS reliability ranging from 68% - 89%. This increase is smallest for the largest horizontal scale of fluctuation, as a weak layer is more likely to cause retrogressive failure and horizontal sliding.

For $\theta_h$ > 24 m, $R_{initial}$ remains constant, whereas $R_{ULS}$ reduces slightly when $\theta_h$ increases from 24 m to 48m. Moreover, even though the increase in reliability is lowest for $\theta_h$ = 48 m, the lowest reliability against ULS failure still occurs for $\theta_h$ = 12 m, due to the lower reliability against initial failure, i.e. the $R_{ULS}$ pattern is very similar to the $R_{initial}$ pattern. Investigation for different factors of safety, i.e. different overall reliability of the dyke, into the effect of $\theta_h$ on $R_{initial}$ and $R_{ULS}$ is required to obtain a clear understanding of the effect of residual dyke strength. The $\theta_h$ at which the reliability is minimum, located in this analysis at $\theta_h$ = 12 m, is expected to change for different factors of safety. Therefore it is necessary to keep investigating multiple horizontal scales of fluctuation in future research.

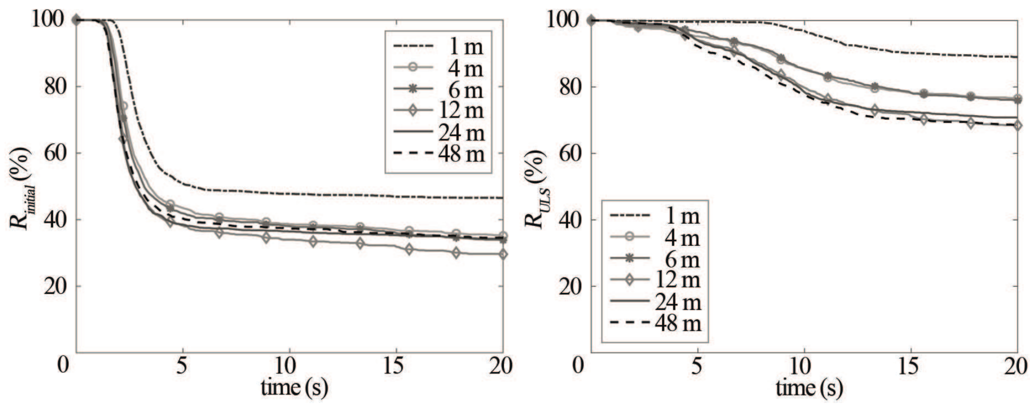


**Figure 6.** Development of reliability over time: (a) reliability against initial failure (without residual dyke strength); (b) reliability against ULS failure (with residual dyke strength).

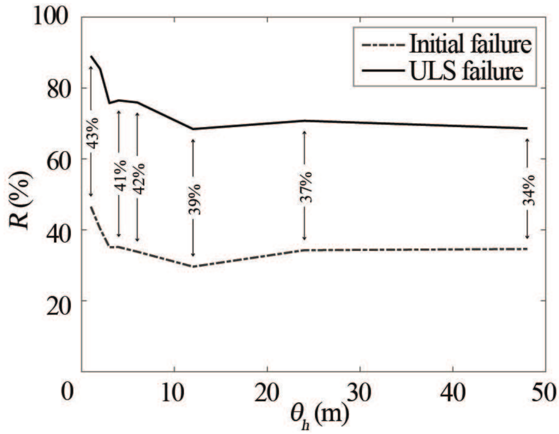


**Figure 7.** Effect of horizontal scale of fluctuation on initial and ULS reliability at end of simulations.

## 7 Conclusions

MPM has been shown to be capable of modelling multiple types of dyke failure macro-instabilities. Both rotational slope and horizontal slide failure mechanisms have been computed with deterministic and stochastic (RMPM) frameworks. While the effect of the residual dyke strength was limited in the deterministic analysis, a significant increase in reliability can be achieved by taking residual dyke strength into account with RMPM. However, further investigation is required to fully understand the effect of spatial variability on residual dyke strength. These simulations have not been based on real dykes, and due to the many simplifications the results are meant only to indicate the capabilities of the model and develop hypotheses for further investigations.

**Acknowledgments**

This work is part of the research programme AllRisk which is financed by the Netherlands Organisation for Scientific Research (NWO), project number P15-21 Project 4.

## References

Bing, Y., Cortis, M., Charlton, T.J., Coombs, W.M., and Augarde, C.E. (2019). B-spline based boundary conditions in the material point method. *Computers and Structures*, 212, 257–274.

Gonzalez Acosta, J.L., Vardon, P.J., and Hicks, M.A. (2017). An evaluation of MPM, GIMP and CMPM in geotechnical problems considering large deformations. *Proc., Fifteenth International Conference of the International Association for Computer Methods and Advances in Geomechanics*, Wuhan, China.

Griffiths, D.V., Huang, J., and Fenton, G.A. (2009). Influence of spatial variability on slope reliability using 2D random fields. *Journal of Geotechnical and Geoenvironmental Engineering*, 135(10), 1367–1378.

MIM (2016). *Schematiseringshandleiding macrostabiliteit – WBI 2017*, Technical Report. Ministerie van Infrastructuur en Milieu, The Netherlands.

Remmerswaal, G. (2017). *Development and Implementation of Moving Boundary Conditions in the Material Point Method.* MSc Thesis, Faculty of Civil Engineering and Geosciences, Delft University of Technology, Delft, The Netherlands.

Remmerswaal, G., Hicks, M.A., and Vardon, P.J. (2018). Ultimate limit state assessment of dyke reliability using the random material point method. *Proc., Fourth International Symposium on Computational Geomechanics*, Assisi, Italy, 89–90.

Sulsky, D., Chen, Z., and Schreyer, H.L. (1994). A particle method for history-dependent materials. *Computer Methods in Applied Mechanics Engineering*, 118(1–2), 179–196.

’t Hart, H., De Bruijn, R., and de Vries, G. (2016). *Fenomenologische beschrijving: Faalmechanismen WTI (translated in English: Phenomenological description: Failure mechanisms WTI)*, technical report, Rijkswaterstaat Water, Verkeer en Leefomgeving, The Netherlands.

Van Baars, S. (2004). Dutch dyke breach, Wilnis 2003. *Proc., Fifth International Conference on Case Histories in Geotechnical Engineering*, New York, USA, 1–4.

Van Baars, S. (2005). The horizontal failure mechanism of the Wilnis peat dyke. *Géotechnique*, 55(4), 319–323.

Varkey, D., Hicks, M.A., and Vardon, P.J. (2018). 3D slope stability analysis with spatially variable and cross-correlated shear strength parameters. *Proc., Ninth European Conference on Numerical Methods in Geotechnical Engineering*, CRC Press/Balkema – Taylor & Francis Group, Leiden, The Netherlands, 543–548.

Wang, B., Hicks, M.A., and Vardon, P.J. (2016). Slope failure analysis using the random material point method. *Géotechnique Letters,* 6(2), 113–118.